PHYSICAL REVIEW D **78,** 054506 (2008)

Impact of dynamical fermions on QCD vacuum structure

Peter J. Moran and Derek B. Leinweber

Special Research Centre for the Subatomic Structure of Matter (CSSM), Department of Physics, University of Adelaide 5005, Australia

(Received 15 January 2008; published 15 September 2008)

We examine how dynamical fermions affect both the UV and infrared structure of the QCD vacuum. We consider large $28^3 \times 96$ lattices from the MILC collaboration, using a gluonic definition of the topological charge density, founded on a new over-improved stout-link smearing algorithm. The algorithm reproduces established results from the overlap formalism and preserves nontrivial topological objects, including instantons. At short distances we focus on the topological charge correlator, $\langle q(x)q(0)\rangle$, where negative values at small x reveal a sign-alternating layered structure to the topological-charge density of the QCD vacuum. We find that the magnitudes of the negative dip in the $\langle q(x)q(0)\rangle$ correlator and the positive $\langle q(0)^2\rangle$ contact term are both increased with the introduction of dynamical fermion degrees of freedom. At large distances we examine the extent to which instanton-like objects are found on the lattice, and how their distributions vary between quenched and dynamical gauge fields. We show that dynamical gauge fields contain more instanton-like objects with an average size greater than in the quenched vacuum. Finally, we directly visualize the topological charge density in order to investigate the effects of dynamical sea-quark degrees of freedom on topology.

DOI: 10.1103/PhysRevD.78.054506 PACS numbers: 12.38.Gc, 11.15.Ha, 12.38.Aw

I. INTRODUCTION

The study of QCD vacuum structure is one area of research where lattice simulations provide access to otherwise inaccessible information. By generating typical vacuum gauge field configurations we are able to directly investigate their complex structure. Further, by varying the simulation parameters we can assess how different physical phenomena contribute to the structure of the vacuum. In particular, we are able to examine the effect of dynamical sea-quarks on the QCD vacuum.

A study of QCD vacuum structure at different scales usually requires the use of a filtering procedure. By removing the short-range UV fluctuations, one can probe the long-distance structural features of the vacuum. Typical UV filtering methods include cooling [1–3], APE [4,5], and improved APE smearing [6], HYP smearing [7] and more recently, stout-link smearing [8–10] and LOG smearing [11]. More recently, the truncation of a spectral representation of operators using eigenmodes of the overlap Dirac operator has been explored as a method to remove UV fluctuations [12–15].

In this paper we investigate the structure of the QCD vacuum on both short and long distance scales using over-improved stout-link smearing [9,10] and a highly-improved measure of the topological charge density [16]. The stability of instanton-like objects under over-improved stout-link smearing [10] allows us to achieve the most accurate determination of instanton size distributions to date.

In addition, Ilgenfritz, *et al.* [14] have recently demonstrated the strong correlation between over-improved stout-link smearing and the truncated overlap Dirac operator. To good accuracy, the UV-cutoff in the Dirac operator is directly related to the number of over-improved stout-link smearing sweeps. However, the overlap Dirac operator is computationally expensive and not suited for high-statistics studies on large dynamical gauge fields. Over-improved stout-link smearing therefore provides the most accurate technique for studying both quenched and dynamical gauge fields with statistics sufficient to reveal differences in the vacuum structure.

On short distance scales one studies vacuum structure through an analysis of the topological charge density correlator, or Euclidean 2-point correlation function

$$\langle qq\rangle \equiv \langle q(x)q(0)\rangle, \tag{1}$$

which is the integrand of the topological susceptibility

$$\chi \equiv \frac{\langle Q^2\rangle}{V} = \int d^4x \langle q(x)q(0)\rangle, \tag{2}$$

where V is the 4-volume. Recent overlap results [13,17] have detailed the strong negative behavior of the 2-point function in quenched gauge fields. Reference [14] demonstrated how it is also possible to generate a strong negative correlator using five sweeps of over-improved stout-link smearing.

However, these studies have all been on quenched gauge fields. There have been no studies of the differences between quenched and dynamical fields in the short-distance correlator [18]. This paper will address this issue with a high-statistics study on several accurately matched large volume lattices from MILC [20,21] using the accurate over-improved stout-link smearing algorithm.

This paper is organized as follows. In Sec. II we provide a brief explanation of over-improved stout-link smearing and direct the reader elsewhere [10] for the full details. In Sec. III, we examine the shapes of the $\langle qq\rangle$ correlator using

over-improved stout-link smearing. We use the gluonic definition of the topological charge density

$$q(x) = \frac{g^2}{32\pi^2}\epsilon_{\mu\nu\rho\sigma}\,\mathrm{Tr}[F_{\mu\nu}(x)F_{\rho\sigma}(x)], \tag{3}$$

where

$$Q = \sum_x q(x), \tag{4}$$

and $F_{\mu\nu}(x)$ is a 3-loop improved field strength tensor [16]. Here we focus on the short-distance structure of the correlator and the role of dynamical fermion degrees of freedom.

In Sec. IV we probe the infrared structure of the full dynamical QCD vacuum. We examine the extent to which instantons are found in the QCD vacuum and how the extra dynamical fermion degrees of freedom affect their distribution throughout the vacuum.

Finally, in Sec. V we directly visualize the topological charge density in order to investigate the effects of dynamical sea-quark degrees of freedom on topology. Conclusions are summarized in Sec. VI.

II. SIMULATION DETAILS

Standard stout-link smearing, using an isotropic smearing parameter ρ_{sm}, involves a simultaneous update of all links on the lattice. Each link is replaced by a smeared link $\tilde{U}_\mu(x)$

$$\tilde{U}_\mu(x) = \exp(iQ_\mu(x))U_\mu(x), \tag{5}$$

where

$$Q_\mu(x) = \frac{i}{2}(\Omega_\mu^\dagger(x) - \Omega_\mu(x)) - \frac{i}{6}\,\mathrm{Tr}(\Omega_\mu^\dagger(x) - \Omega_\mu(x)), \tag{6}$$

with

$$\Omega_\mu(x) = \rho_{\mathrm{sm}}\sum\{1\times 1 \text{ loops involving } U_\mu(x)\}. \tag{7}$$

The over-improvement parameter ϵ is introduced into the smearing process by replacing the combination of links in $\Omega_\mu(x)$ with

$$\Omega_\mu(x) = \rho_{\mathrm{sm}}\sum\Big\{\frac{5-2\epsilon}{3}(1\times 1 \text{ loops involving } U_\mu(x)) - \frac{1-\epsilon}{12}(1\times 2 + 2\times 1 \text{ loops involving } U_\mu(x))\Big\}. \tag{8}$$

Note that both forward and backward horizontally orientated rectangles are included in the 2×1 loops, such that $\Omega_\mu(x)$ resembles the local action.

The parameter ϵ is tuned to preserve instanton-like objects in the gauge field. As detailed in Ref. [10], a value of $\epsilon = -0.25$ is optimal for preserving topological objects and their properties. With this extended link path and value of ϵ, we take $\rho_{\mathrm{sm}} = 0.06$, smaller than the standard value of 0.1. A full derivation and explanation of the benefits of over-improved smearing is provided in Ref. [10].

TABLE I. The gauge fields used in this study. The lattices were generated by the MILC collaboration [20,21]. In the following we refer to these ensembles as "quenched," "heavy," and "light."

Size	β	a	Bare Quark Masses
$28^3\times 96$	8.40	0.086 fm	∞
$28^3\times 96$	7.11	0.086 fm	27.1 MeV, 67.8 MeV
$28^3\times 96$	7.09	0.086 fm	14.0 MeV, 67.8 MeV

The gauge fields for this study were generated by the MILC collaboration [20,21] using a Tadpole and Symanzik improved gauge action with $1\times 1 + 1\times 2 + 1\times 1\times 1$ terms in the quenched case and an Asqtad staggered dynamical fermion action for the $2+1$ flavors of dynamical quarks. The lattice spacing for all three types of gauge fields is $a = 0.086$ fm. For the specifics of how the gauge fields were generated see Refs. [20,21]. Simulation parameters are summarized in Table I.

III. TOPOLOGICAL CHARGE DENSITY CORRELATOR

The Euclidean 2-point correlation function for the topological charge $q(x)$

$$\langle qq\rangle \equiv \langle q(x)q(0)\rangle, \tag{9}$$

also known as the topological charge density correlator, is negative for any $x > 0$ [22,23]. This follows simply from reflection positivity [17]. Given that the correlator must have a positive contact term $\langle q^2(0)\rangle_x$, the correlator necessarily has the form

$$\langle q(x)q(0)\rangle = A\delta(x) - f(x), \tag{10}$$

where $f(x)$ is necessarily positive for all x away from the origin.

Recent studies [13,17] of vacuum structure using the overlap-defined topological charge density have demonstrated the strong negativity of the topological charge density correlator in lattice simulations. This strong negative behavior was also observed using the gluonic definition of Eq. (3) in Ref. [14]. The negative behavior of the $\langle qq\rangle$ correlator suggests a sign-alternating layered structure to the topological charge density of the topological charge density correlator.

We begin our study by investigating the effects of dynamical sea-quark degrees of freedom on the topological charge density. In quenched QCD the Witten-Veneziano [24,25] formula gives a relation between the topological susceptibility and the mass of the η' meson [22]

$$\chi^{\mathrm{qu}} = \frac{m_{\eta'}^2 F_\pi^2}{2N_f}. \tag{11}$$

However, in the full dynamical case the topological susceptibility should vanish in the chiral limit [22,26]

$$\chi^{\mathrm{dyn}} = \frac{f_\pi^2 m_\pi^2}{2N_f} + \mathcal{O}(m_\pi^4). \tag{12}$$

Of course, a vanishing topological susceptibility puts no restraints on how the function $\langle q(x)q(0)\rangle$ should change with the addition of dynamical sea-quarks, it only requires that the integral in Eq. (2) vanishes.

It is well known that the inclusion of dynamical sea-quarks in the QCD action renormalizes the coupling constant. In order to maintain the same lattice spacing across quenched and dynamical gauge fields, one finds that the coupling parameter, g, must increase and hence $\beta \sim 1/g^2$ must be smaller for the dynamical fields.

In quenched QCD it is possible to make a prediction on how the amplitude of the delta function, A, of Eq. (10) should change as β is altered. In the quenched QCD action formulated in Euclidean space, β appears as a factor governing the width of the probability distribution for gauge-field links. When generating quenched gauge fields, the smaller β values will permit greater fluctuations in the gauge links. The increased fluctuations can give rise to nontrivial field fluctuations, which will be manifest through a greater mean-square topological-charge density $\langle q^2(0)\rangle_x$, and thus a larger A.

However, in full QCD the probability distribution is now proportional to $e^{-S_{\mathrm{Eff}}}$, where $S_{\mathrm{Eff}} = S_G + \ln \det[M]$ and M denotes the fermion interaction matrix. Since M depends on both the link variables and the quark masses, it is no longer evident that smaller β values will allow larger fluctuations in the gauge links relative to quenched QCD. Although one cannot predict a change in the mean-square density, we can make the following observation. As one approaches the chiral limit $\chi^{\mathrm{dyn}} \to 0$, it follows from Eq. (12) that an increasing (decreasing) mean-square density $\langle q^2(0)\rangle_x$ must be compensated for by a stronger (shallower) negative dip in the $\langle qq\rangle$ correlator.

Figure 1 examines the extent to which the local field fluctuations differ through a comparison of the $\langle qq\rangle$ correlator for the quenched and two dynamical ensembles. These correlators were generated after using five sweeps of over-improved stout-link smearing to suppress otherwise large renormalizations. We see that the contact term $\langle q^2(0)\rangle_x$ is in fact larger, and the magnitude of the negative dip has also increased. These effects are also stronger for lighter quark masses. This is consistent with our reasoning from considerations of quenched QCD. Smaller quark masses require smaller β values. The exact values of the positive contact term are; quenched $= 1836 \pm 3$ fm^{-8}, heavy $= 3344 \pm 5$ fm^{-8}, light $= 3443 \pm 4$ fm^{-8}.

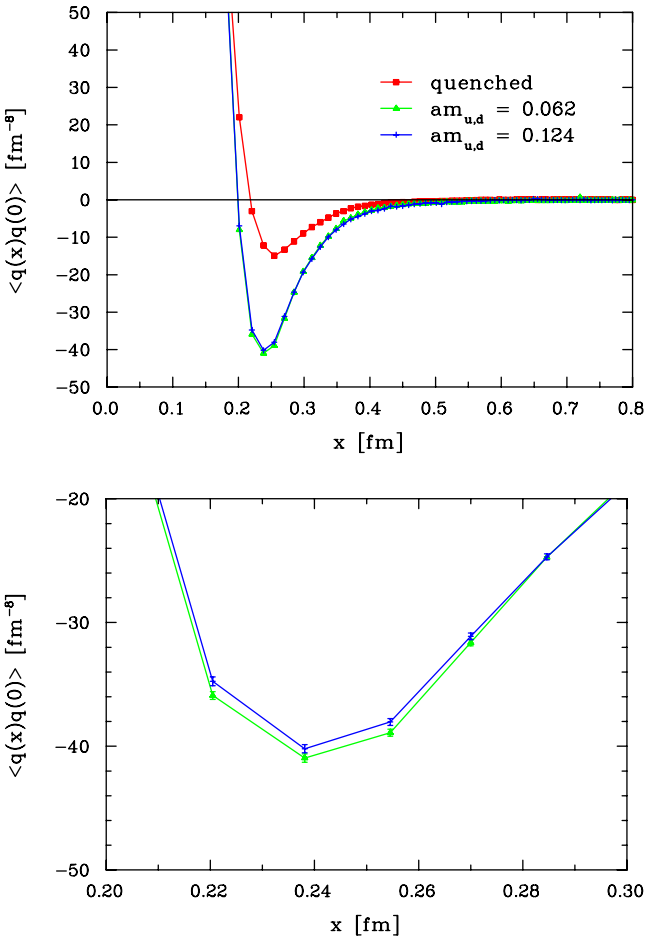

FIG. 1 (color online). A comparison of the $\langle qq\rangle$ correlator for quenched and dynamical gauge fields. The greater field fluctuations present in the dynamical fields are visible through an increase in the magnitude of the negative dip. Although not shown, the contact term $\langle q^2(0)\rangle_x$ has also increased and values are given in the text. The lower graph displays the same data focusing on the negative dip for the dynamical fields. The magnitude of the dip is greater for the lighter quark mass.

IV. INSTANTON-LIKE OBJECTS

A. Profile versus charge density

Understanding the nature of instanton-like objects in the QCD vacuum continues to be an active of area of investigation. Considerable UV filtering reveals the presence of long-distance topological structures in the QCD vacuum. While these topological objects are only approximations to the classical instanton solution, they are commonly referred to as (anti-)instantons.

We now proceed to quantitatively analyze the similarity of the topological objects in the QCD vacuum to the classical instanton solution. Using over-improved stout-link smearing we are able to extract both the action and charge densities of our gauge fields. Starting with the action density we locate the positions of all local maxima

in the field. The local maxima are identified by finding a point at the center of a 3^4 hypercube whose action density exceeds that of the neighboring 80 points of the hypercube.

Taking each maxima to be the approximate center of a possible instanton-like object we fit the classical instanton action density

$$S_0(x) = \xi \frac{6}{\pi^2} \frac{\rho_{\text{inst}}^4}{((x - x_0)^2 + \rho_{\text{inst}}^2)^4}, \tag{13}$$

to the measured action density. An arbitrary scale factor, ξ, is included to allow the *shape* of the action density to determine the size, ρ_{inst}. We fit the six parameters ξ, ρ_{inst}, and the four components of x_0 by fitting Eq. (13) to the action density of the aforementioned 3^4 hypercube.

From ρ_{inst} one can infer the topological charge to be observed at the center of the distribution $q(x_0)$ if it truly is an instanton

$$q(x_0) = Q \frac{6}{\pi^2 \rho_{\text{inst}}^4}. \tag{14}$$

Here $Q = \pm 1$ for an instanton/anti-instanton. This can then be compared with the topological charge measured directly from the charge density observed on the lattice.

For this part of the investigation we use 45 sweeps of over-improved stout-link smearing. This corresponds to a λ_{cut} of 634 MeV in the truncated overlap operator [14]. A calculation of $q(x_0)$ on the "light" ensemble of dynamical gauge fields (with $\beta = 7.09$) is provided in Fig. 2. With the exception of only two outliers, the maxima are good local approximations to the classical instanton solution.

While the centers of the instanton-like objects resemble instantons, it is interesting to assess how similar the remainder of the instanton-like objects are to a classical instanton. To do so, we consider all points within a distance

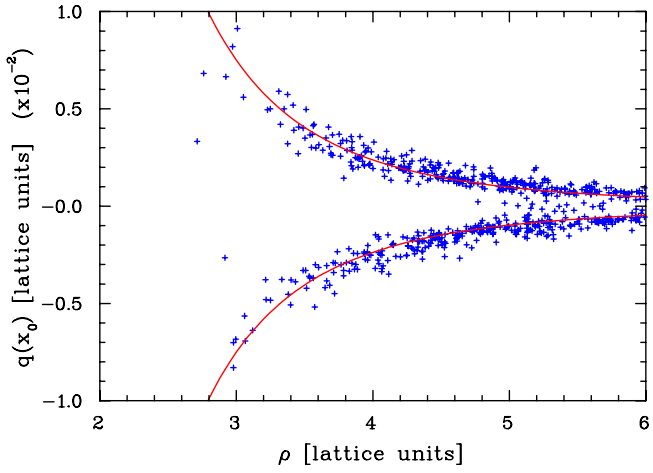

FIG. 2 (color online). Comparison of the calculated $q(x_0)$ after 45 sweeps of smearing with the exact instanton solution. After 45 sweeps of smearing the majority of topological objects are relatively good approximations to instantons at their cores.

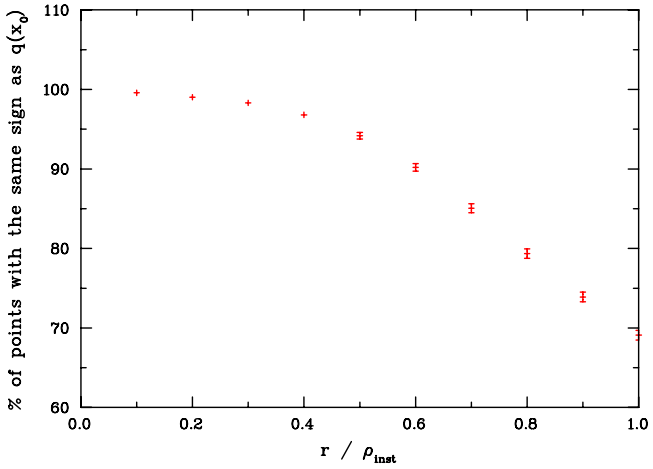

FIG. 3 (color online). The percentage of points that are sign coherent within a relative distance r/ρ_{inst} of each instanton-like objects' center x_0 with size ρ_{inst}. For small r/ρ_{inst} the percentage of sign-coherent points is close to 100, however the sign-coherence falls off rapidly as r approaches the characteristic size ρ_{inst}.

r from the center x_0, measured relative to the instanton size ρ_{inst}, and examine the extent to which the points within this distance have the same sign topological-charge density as observed at the center, $q(x_0)$. If the detected object is a good approximation to a classical instanton then all these points should have the same charge as $q(x_0)$.

In Fig. 3 we show the percentage of points that are within a relative distance r/ρ_{inst} of x_0 that have the same sign as x_0. For small r/ρ_{inst} the percentage of sign-coherent points is close to 100, however it falls off rapidly as r approaches the characteristic size ρ_{inst}. This suggests that although the object is representative of an instanton at its center, the tails of the objects are distorted by vacuum fluctuations. What is remarkable is that at the characteristic size of the "instanton," merely 2/3 of the points are sign coherent, suggesting that the objects revealed after 45 sweeps of smearing are good approximations of classical instantons only at the core.

B. Dynamical fermions and instanton structure

Given the strong correlation between $q(x_0)$ extracted from the action density after 45 sweeps of smearing and that given by the classical solution (14) we can now compare "instanton" distributions between quenched and dynamical QCD.

Early attempts [27] to reveal differences in the distributions were limited by statistical fluctuations, concluding that the differences must be subtle. However, this high-statistics study exploiting the accuracy of over-improved stout-link smearing is able to resolve differences for the first time.

To examine the variation in instanton size between the different gauge fields, a histogram of ρ_{inst} is presented in

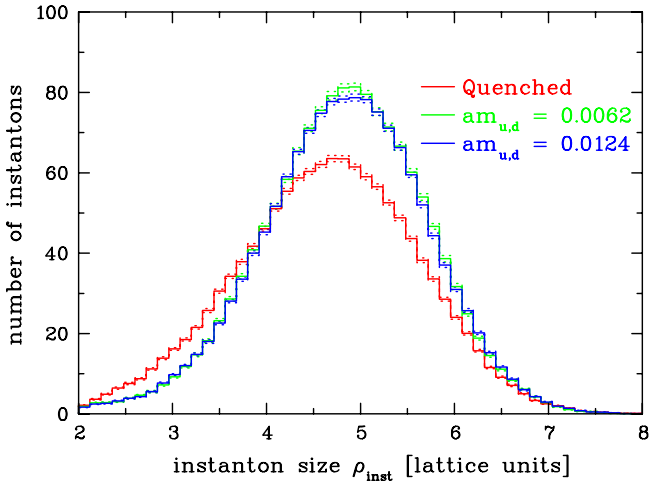

FIG. 4 (color online). Histogram of the instanton size ρ_{inst} in dynamical and quenched gauge fields. The dynamical fields show both an increase in the number of instantons and in the average instanton size.

Fig. 4. Compared to the quenched ensemble, the dynamical gauge fields show a substantial increase in the total number of instantons and a subtle but important increase in average instanton size. Our sample size of 73 000 instantons from quenched QCD and 140 000 from full QCD enables a precise determination of the means of the distributions. We find $\rho_{\text{inst}}(\text{Quenched}) = 4.646(4)$, $\rho_{\text{inst}}(\text{am}_{u,d} = 0.0062) = 4.822(4)$, and $\rho_{\text{inst}}(\text{am}_{u,d} = 0.0124) = 4.825(3)$, and the standard deviations of the distributions to be $\sigma(\text{Quenched}) = 0.96$, $\sigma(\text{am}_{u,d} = 0.0062) = 0.87$, $\sigma(\text{am}_{u,d} = 0.0124) = 0.87$. These results are similar in spirit to our observations of the short-distance $\langle qq \rangle$ correlator in that the introduction of dynamical fermion degress of freedom leads to more nontrivial topological charge fluctuations, at both short and long distances.

It has been argued that an increased density of instanton-like objects on the lattice could be explained through an instanton/anti-instanton attraction occurring due to the presence of the fermion determinant in the QCD weight factor [26]. The idea is that an isolated instanton or anti-instanton would give rise to a near zero mode of the Dirac operator. When generating dynamical gauge fields the selection of typical configurations is weighted by $\det(\not{D} + m)e^{-S_g}$. If a near zero-mode of $\not{D}$ were to exist on the lattice then the determinant would approach 0 in the chiral limit and it would be highly improbable that the configuration would be selected. Thus, isolated instantons are unlikely to exist in the light dynamial-fermion gauge fields and hence all instanton-like objects will be closer in these fields. Combined with our earlier results displaying increased fluctuations in the gauge-field links, these considerations lead one to anticipate a greater number of instanton-like objects in the dynamical gauge fields and an increase in their size to aid in suppressing isolation.

V. TOPOLOGICAL CHARGE DENSITY

The effects of dynamical fermion degrees of freedom are realized significantly at short distances in the calculation of the $\langle qq \rangle$ correlator. The increased magnitude of the nontrivial topological charge field fluctuations that are permitted due to the inclusion of fermion loops should also be visible in direct visualizations of the topological charge density.

Using five sweeps of over-improved stout-link smearing, we consider the short-range structure of the topological charge density. In Fig. 5 we present the topological charge density for the quenched and two dynamical ensembles. The extra field fluctuations are clearly visible in the visualizations of the dynamical QCD vacuum structure.

In Fig. 6, we compare the structure of the vacuum after 45 sweeps of over-improved smearing as discussed in Sec. IV. It is difficult to observe the increased density of instantons upon the introduction of dynamical fermions in these figures. This is because the charge density fluctuates over a long times scale and a single time-slice is insufficient to portray an complete representation of the vacuum. We also note that despite the apparent separation of these topological lumps in the vacuum, all regions of like charge are connected throughout the gauge field; i.e. one can

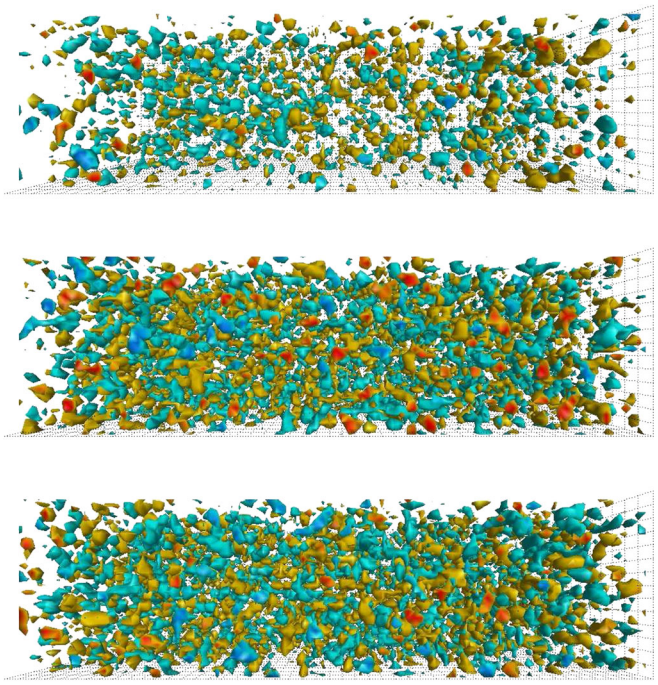

FIG. 5 (color online). The topological charge density for the quenched and dynamical ensembles, obtained after five sweeps of over-improved stout-link smearing. From top to bottom we plot a quenched field, the heavy dynamical $am_{u,d} = 0.0124$, $am_s = 0.031$ field and the light dynamical $am_{u,d} = 0.0062$, $am_s = 0.031$ field. The greater nontrivial field excitations that are permitted upon the introduction of light dynamical fermions are directly visible in the dynamical illustrations.

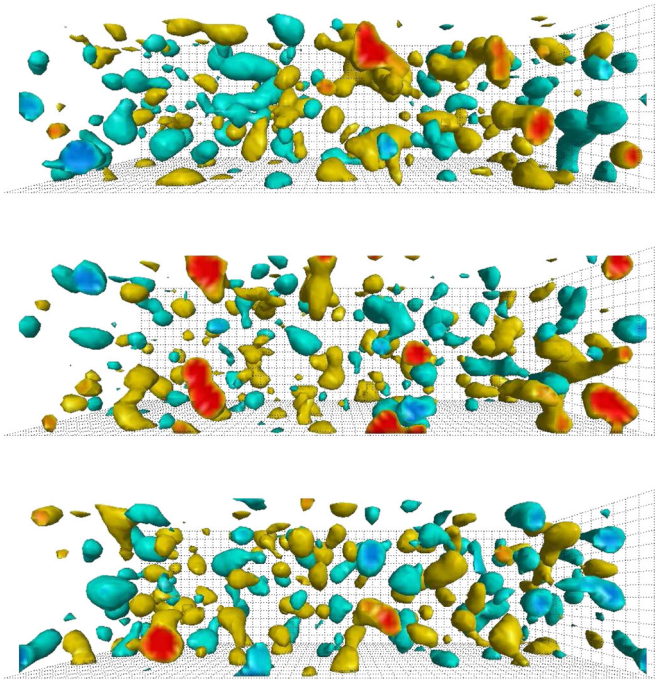

FIG. 6 (color online). The topological charge density for the quenched and dynamical ensembles, obtained after 45 sweeps of over-improved stout-link smearing. From top to bottom we plot a quenched field, the heavy dynamical $am_{u,d} = 0.0124$, $am_s = 0.031$ field and the light dynamical $am_{u,d} = 0.0062$, $am_s = 0.031$ field. The longer correlation length makes it difficult to observe a noticeable difference in the size-distribution of the gauge field fluctuations when observing a single time-slice.

travel from one lump to any other lump of the same charge along a sign-coherent path of small-magnitude topological-charge density. This has been examined in detail elsewhere [17,28].

VI. CONCLUSION

Using the new over-improved stout-link smearing algorithm we are able to perform the most accurate studies of QCD vacuum structure to date. The use of this smearing algorithm allows one to accurately expose the differences between quenched and dynamical fields on both long and short-distance scales.

By suppressing large renormalizations of the lattice operators through five sweeps of over-improved stout-link smearing on the gauge fields, which corresponds to the unfiltered overlap operator [14], we are able to demonstrate how dynamical fermions affect the vacuum through a calculation of the topological charge density correlator. The addition of fermions into the QCD action at constant lattice spacing renormalizes the coupling constant such that the coupling parameter β becomes smaller. In the quenched approximation such a change permits greater field fluctuations, and this is realized in full QCD. We find an increase in the mean-square topological charge density upon including dynamical fermions, as is illustrated in Fig. 1. The larger contact term, reflecting the greater mean-square topological charge density of dynamical configurations, also induces an increase in the negative dip of the topological charge density correlators. The strength of these compensating effects is expected to increase as one approaches the chiral limit.

The results also reflect the suppression of zero modes due to the inclusion of the $\det(\not{\partial} + m)$ weight factor in the selection of typical gauge fields, resulting in a decrease in the number of isolated instanton-like objects. This causes instantons and anti-instantons to be ''attracted'' [26] and leads to an increase in both the density and size of instanton-like objects in the dynamical gauge fields and illustrated in Figs. 4 and 5.

These results support the emerging picture of the vacuum as an alternating ''sandwich'' of opposite topological charge density [17]. Beneath this oscillating short-range structure there exists a long-distance foundation of instanton-like objects [13,29,30] that can be revealed through smoothing or Dirac eigenmodes [14]. The addition of dynamical fermions allows stronger field fluctuations and a higher frequency of sign-oscillations in the topological charge density. The density of instanton-like objects beneath these short-distance oscillations also increases, as does their average size.

ACKNOWLEDGMENTS

The authors thank Ernst-Michael Ilgenfritz and Waseem Kamleh for constructive and insightful discussions. We also thank the Australian Partnership for Advanced Computing (APAC) and the South Australian Partnership for Advanced Computing (SAPAC) for generous grants of supercomputer time which have enabled this project. This work is supported by the Australian Research Council.

[1] B. Berg, Phys. Lett. **104B**, 475 (1981).
[2] M. Teper, Phys. Lett. **162B**, 357 (1985).
[3] E.-M. Ilgenfritz, M. L. Laursen, G. Schierholz, M. Muller-Preussker, and H. Schiller, Nucl. Phys. **B268**, 693 (1986).
[4] M. Falcioni, M. L. Paciello, G. Parisi, and B. Taglienti, Nucl. Phys. **B251**, 624 (1985).
[5] M. Albanese *et al.* (APE), Phys. Lett. B **192**, 163 (1987).
[6] F. D. R. Bonnet, D. B. Leinweber, A. G. Williams, and J. M. Zanotti, Phys. Rev. D **65**, 114510 (2002).

[7] A. Hasenfratz and F. Knechtli, Phys. Rev. D **64**, 034504 (2001).
[8] C. Morningstar and M. J. Peardon, Phys. Rev. D **69**, 054501 (2004).
[9] P. J. Moran and D. B. Leinweber, Proc. Sci., LATTICE2007 (2007) 383.
[10] P. J. Moran and D. B. Leinweber, Phys. Rev. D **77**, 094501 (2008).
[11] S. Durr, arXiv:0709.4110.
[12] I. Horvath *et al.*, Phys. Rev. D **67**, 011501 (2003).
[13] E. M. Ilgenfritz *et al.*, Phys. Rev. D **76**, 034506 (2007).
[14] E.-M. Ilgenfritz, D. Leinweber, P. Moran, K. Koller, G. Schierholz, and V. Weinberg, Phys. Rev. D **77**, 074502 (2008).
[15] F. Bruckmann, Proc. Sci., LATTICE2007 (2007) 006.
[16] S. O. Bilson-Thompson, D. B. Leinweber, and A. G. Williams, Ann. Phys. (N.Y.) **304**, 1 (2003).
[17] I. Horvath *et al.*, Phys. Lett. B **617**, 49 (2005).
[18] We note the early investigation of the dynamical 2-point function by Hasenfratz [19] on small lattices where 30 sweeps of unimproved APE smearing [6] was applied. This level of smoothing is sufficient to remove most of the short-distance fluctuations which give rise to the negative dip in the correlator. And while a comparison was made between the highly-smoothed quenched and dynamical fields it is impossible to draw any strong conclusions, as the lattice spacings were not matched accurately. It is now well established that the shape of the topological charge density correlator depends significantly on the lattice spacing [13,17].
[19] A. Hasenfratz, Phys. Lett. B **476**, 188 (2000).
[20] C. Aubin *et al.*, Phys. Rev. D **70**, 094505 (2004).
[21] C. W. Bernard *et al.*, Phys. Rev. D **64**, 054506 (2001).
[22] E. Seiler, Phys. Lett. B **525**, 355 (2002).
[23] E. Seiler and I. O. Stamatescu, arXiv:mPI-PAE/PT.
[24] E. Witten, Nucl. Phys. **B156**, 269 (1979).
[25] G. Veneziano, Nucl. Phys. **B159**, 213 (1979).
[26] A. Hart and M. Teper (UKQCD), Phys. Lett. B **523**, 280 (2001).
[27] R. C. Brower, T. L. Ivanenko, J. W. Negele, and K. N. Orginos, Nucl. Phys. B, Proc. Suppl. **53**, 547 (1997).
[28] I. Horvath *et al.*, Phys. Rev. D **68**, 114505 (2003).
[29] P. de Forcrand, in *Quark Confinement and the Hadron Spectrum VII*, edited by J. E. F. T Ribeiro *et al.*, AIP Conf. Proc. No. 892 (AIP, New York, 2007), p. 29.
[30] P. J. Moran and D. B. Leinwber, in QCD Down Under: Proceedings of the Workshop on Quantum Chromodynamics, Adelaide, Australia, 2004, edited by A. Kizilersü, A. W. Thomas, and A. G. Williams (Elsevier, Amsterdam, 2005), p. 777.